PHYSICAL REVIEW D VOLUME 24, NUMBER 5 1 SEPTEMBER 1981

Inclusive study of off-mass-shell $\pi^{\pm}p$ and $\pi^{\pm}\pi^{-}$ interactions

F. Barreiro,* O. Benary,† E. S. Hafen, R. I. Hulsizer, V. Kistiakowsky, J. B. McManus, A. Napier,‡ I. A. Pless, J. P. Silverman,§ P. C. Trepagnier,‖ J. Wolfson,¶ and R. K. Yamamoto

Department of Physics and Laboratory for Nuclear Science, Massachusetts Institute of Technology, Cambridge, Massachusetts 02139

(Received 29 December 1980)

We have studied inclusive ρ^0 and Δ^{++} production in π^+p and π^-p interactions at 15 GeV/c in a region where pion exchange has been found to dominate the resonance production. By using ρ^0 production, the off-mass-shell interactions of virtual pions with the target protons have been studied and compared with the same on-shell reactions at comparable energy. No significant differences between on-shell and off-shell reactions have been found in topological-cross-section ratios, inclusive longitudinal- or transverse-momentum distributions, or elastic $d\sigma/dt$ distributions. The effect of the negative mass squared of the virtual pions has also been studied. Inclusive Δ^{++} production has been found to be dominated by pion exchange for $|t| \lesssim 0.4$ (GeV/c)^2. We have studied the interactions of these off-shell pions with the beam pions as a function of energy. The ratio σ_{el}/σ_T and the average charged-particle multiplicities $\langle n_X \rangle$ have been examined and compared with those for various hadron-proton reactions. The values of $\langle n_X \rangle$ have also been studied in terms of a simple model and found to give results consistent with studies at higher energies. We also present longitudinal- and transverse-momentum distributions for produced pions, as well as $d\sigma/dt$ distributions for $\pi\pi$ elastic scattering.

I. INTRODUCTION

Although the study of pion-pion interactions has been of interest for many years, the studies of off-mass-shell interactions performed to date have been rather limited in scope, falling into two general categories. In one approach, total and elastic $\pi\pi$ cross sections and elastic-scattering phase shifts are determined by extrapolation to the pion pole, according to the prescriptions of Chew and Low[1] or others.[2] The second approach, less formal and more phenomenological in nature, involves finding reactions in which pion exchange is expected to be the dominant mechanism and studying the interactions of the exchanged pions with real particles. Some studies[3-6] of this type have examined average charged-particle multiplicities; others[6-10] have looked at longitudinal-momentum distributions of the particles produced in such reactions. None of these studies, however, has systematically examined inclusive off-shell reactions.

The purpose of this study is twofold. First, we systematically study off-shell πp interactions in detail and compare them with the same on-shell reactions in order to determine whether or not significant differences exist between on-shell and off-shell particle production. Pion exchange in the reactions

$$\pi^+p \rightarrow \rho^0 + X^{++} \tag{1}$$

and

$$\pi^-p \rightarrow \rho^0 + X^0 \tag{2}$$

at 15 GeV/c is used as a source of off-shell pions, and a cut on the mass of the systems X^{++} and X^0 allows comparison with on-shell data at 3.9 GeV/c. Since the four-momentum transfer t from incoming π to ρ^0 is the (negative) mass squared of the virtual π, cuts in t are used to study the effect of more massive pions.

The second purpose of this work is to study pion-pion interactions and determine which characteristics of such interactions are common to hadron-hadron interactions in general, and which are unique to pion-pion interactions. We use the pion-exchange component of the reactions

$$\pi^+p \rightarrow \Delta^{++} + X^0 \tag{3}$$

and

$$\pi^-p \rightarrow \Delta^{++} + X^{--} \tag{4}$$

as a source of off-shell pions for this study. Cuts in the mass of the systems X^0 and X^{--} provide information about the energy dependence of pion-pion interactions. We present inclusive distributions in both longitudinal- and transverse-momentum for pions produced in such interactions, as well as average charged-particle multiplicities and relative topological cross sections. The $\pi\pi$ elastic-scattering $d\sigma/dt$ distributions are also studied.

The next section of this paper describes the experiment and the data analysis. The third section presents the comparison of on-shell and off-shell πp interactions, while the fourth section presents the results of our study of $\pi\pi$ interactions. In the final section we summarize our results.

II. DATA ANALYSIS

The data for this study come from exposures of the SLAC 82-in. hydrogen bubble chamber to both positive- and negative-pion beams at 15 GeV/c, consisting of approximately 866 000 π^+p pictures and 470 000 π^-p pictures. The π^+p film was measured on the Columbia University Hough-Powell Device, with track reconstruction and kinematic fitting performed at Columbia by the programs TVGP and SQUAW, respectively.[11] The π^-p film was measured on the MIT precision-encoding pattern-recognition (PEPR) system, with reconstruction done by the program GEOMAT and kinematic fitting done by SQUAW.[12,13] In both data sets, all outgoing tracks were assumed to be either protons or pions.

A fraction of the film from both data sets was rescanned in order to determine scanning efficiencies. Cross sections were then calculated and found to be in excellent agreement with the results of high precision counter experiments. Topologically dependent weighting factors were calculated to correct for scanning and processing losses.

Low-momentum protons were identified by their relative ionization. In the π^+p data, scanners selected which track (if any) of an event was a proton with about 90% accuracy up to about 1.2 GeV/c. In half of the π^-p data, scanners identified protons up to 1.0 GeV/c, while in the remaining π^-p data, the ionization of tracks up to 1.2 GeV/c was measured by PEPR.

Kinematic fits (using SQUAW) were made and were used primarily for particle identification in events in which no proton was identified by ionization. A total of 490 655 π^+p events and 146 334 π^-p events were fitted successfully. In cases of ambiguous SQUAW fits, a single fit was selected for this analysis by a series of tests, considering first the proton identification, then the constraint classes of the fits, the momenta of unidentified "protons," and the χ^2 values for the fits. In some cases, fits were chosen randomly. Complete details about the fit-selection criteria may be found elsewhere.[13] Once a fit was selected, the corresponding measured (not fitted) values of momentum and energy were used for this analysis. Thus, the fits were used primarily for particle identification in events in which no proton was identified by ionization.

III. INCLUSIVE ρ^0 PRODUCTION AND OFF-SHELL πp INTERACTIONS

Before looking at off-shell pion-pion interactions, it is first appropriate to study off-shell pions and see if they behave like on-shell pions. Fortunately, a situation exists in which a phenomenological comparison of on-shell and off-shell pion interactions can be made.

A recent study[7] of inclusive ρ^0 production at 15 GeV/c has found pion exchange to be the dominant production mechanism in the beam-fragmentation region. In particular, at values of the Feynman scaling variable x greater than 0.5, the helicity-0, unnatural-parity-exchange matrix element ρ_{00} was found to have the value $\rho_{00} \simeq 0.7$, demonstrating this dominance. A triple-Regge analysis in the same study also found the exchanged particle trajectory to be consistent with that of the pion. One may therefore consider the diagram shown in Fig. 1(a) to be appropriate in this region, and the interactions at the lower vertex of this diagram may be viewed as the reactions

$$\pi^+p \to X \tag{5}$$

and

$$\pi^-p \to X \tag{6}$$

with the pion being off-shell.

In earlier work at MIT,[14,15] reactions (5) and (6) have been studied, on-shell, with incident-pion-

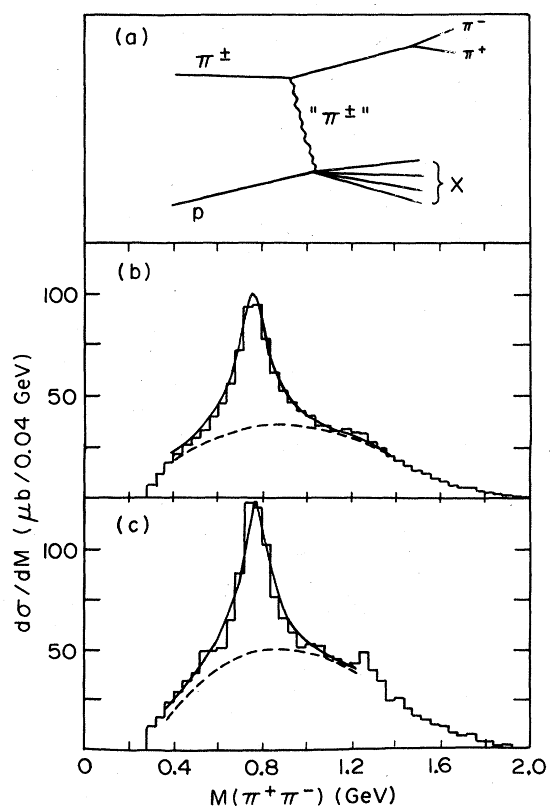

FIG. 1. (a) Feynman diagram for inclusive ρ^0 production by pion exchange. (b) and (c) $\pi^+\pi^-$ effective-mass distributions for $\pi^+p \to \pi^+\pi^- + X$ and $\pi^-p \to \pi^+\pi^- + X$, respectively, in the cuts $x(\pi^+\pi^-) > 0.5$ and $6.8 < M_X^2 < 9.8$ GeV^2. The solid lines show the results of fits (see text); the dashed lines are the contributions from background.

beam momentum of 3.9 GeV/c, corresponding to total center-of-mass energy squared of $s \simeq 8.2$ GeV^2. To make an appropriate comparison with the on-shell data, events of the form

$$\pi p \to \pi^+\pi^- X \tag{7}$$

at 15 GeV/c were selected so as to have an $M_X{}^2$ distribution centered about 8.2 GeV^2 (where M_X is the effective mass of the system recoiling against the $\pi^+\pi^-$ pair which makes up the ρ^0). A cut of $6.8 < M_X{}^2 < 9.8$ GeV^2 was used to provide adequate statistics. In addition, we used the cut of Feynman $x(\pi^+\pi^-) > 0.5$ in order to be in the pion-exchange region. The resulting x distribution was a single large peak in the range $0.5 < x < 0.7$. In cases in which more than one $\pi^+\pi^-$ combination in a given event fell into this cut, the combination whose effective mass was closest to the ρ^0 mass of 770 MeV was chosen.

The effective-mass distributions of such $\pi^+\pi^-$ systems are shown in Figs. 1(b) and 1(c). A large ρ^0 peak can be seen above background in both the π^+p and π^-p data. We have fit these distributions to the sum of a Breit-Wigner mass shape and a polynomial background. The results are shown as the solid curves in Figs. 1(b) and 1(c); the dashed curves represent the contributions of the background. We have defined the ρ^0 region by the cut $620 < M(\pi^+\pi^-) < 920$ MeV. In the π^+p data, this ρ^0 band contains 533 μb, of which 252 ± 16 μb have been determined to be background. In the π^-p data, the background has been found to comprise 358 ± 19 μb out of a total of 666 μb in the ρ^0 band. Narrower mass cuts have also been studied, and the results presented below have been found to be very insensitive to the width of the cut. When a cut on t (from beam to ρ^0) was performed to look at events with different mass virtual pions, a new $\pi^+\pi^-$ mass distribution was generated, and new fits performed.

Because such a large fraction of the data in the ρ^0 band is background, we have performed background subtraction to obtain our results. The background has been modeled by studying events in the x cut described above with either $400 < M(\pi^+\pi^-) < 560$ MeV or $1000 < M(\pi^+\pi^-) < 1160$ MeV. All distributions have been obtained separately for events in the ρ^0 and background bands, with the background distributions being normalized to the area in the ρ^0 mass cut under the polynomials in the fits described above before being subtracted from the ρ^0 band distributions. In performing the subtraction, the statistical uncertainties of both the total ρ^0 band distributions and the background distributions were considered, along with the uncertainty in the amount of background given by the fits. The resulting error bars reflect these uncertainties.

The four-momentum transfer t from beam pion to produced ρ^0 can be interpreted as the (negative) mass squared of the exchanged pion [see Fig. 1(a)]. The t distributions for events in the M_X and x cuts, and in the ρ^0 band, are shown in Fig. 2. To examine the effect of mass on the behavior of the off-shell pions, the t distributions were each divided into three bins with equal statistics, from which three separate sets of distributions were generated. Only small changes in behavior were seen between the ranges of off-shell pion mass. Some distributions were broader or had less pronounced leading peaks (examples are presented later). For the analysis that follows, the three t bins were lumped together to improve statistics.

Unlike real on-shell experiments, the direct calculation of total off-shell πp cross sections is not possible, so that normalization of the off-shell data is necessary. For comparison, all distributions, both on-shell and off-shell, have been normalized by dividing by the total cross sections σ_T. For the on-shell data, the experimental values[14,15] have been used. For the off-shell data, we have

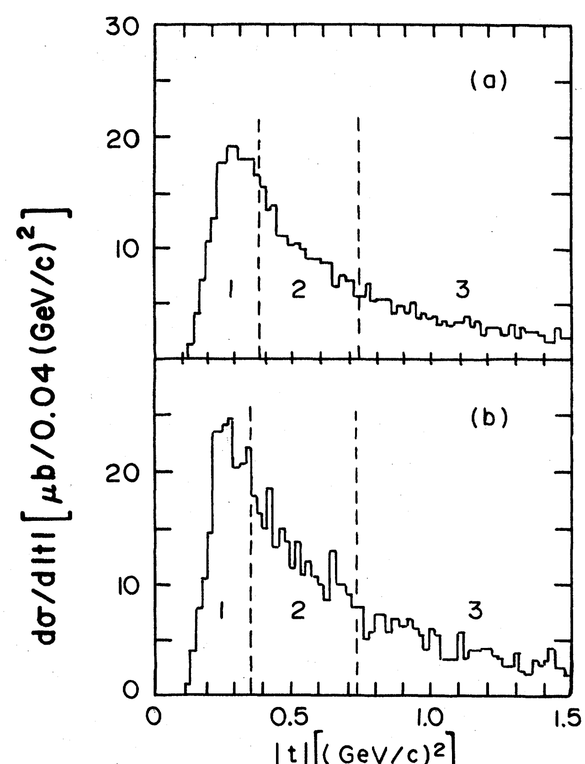

FIG. 2. t (measured from beam to ρ) showing the three t-cut regions (1) $|t| < 0.38$ GeV^2, (2) $0.38 < |t| < 0.74$ GeV^2, (3) $|t| > 0.74$ GeV^2 for (a) $\pi^+p \to \rho^0 + X$, (b) $\pi^-p \to \rho^0 + X$.

TABLE I. Topological-cross-section ratios at 3.9 GeV/c.

n	σ_n/σ_T on-shell	σ_n/σ_T off-shell
	$\pi^-p \to n$ prongs	
0	0.042 ± 0.002	0.048 ± 0.012
2	0.704 ± 0.010	0.648 ± 0.027
4	0.244 ± 0.009	0.276 ± 0.024
6	0.010 ± 0.001	0.021 ± 0.007
	$\pi^+p \to n$ prongs	
2	0.620 ± 0.044	0.591 ± 0.026
4	0.356 ± 0.046	0.372 ± 0.025
6	0.024 ± 0.003	0.036 ± 0.009

defined σ_T as the ρ^0 cross section above background in the mass cut, x cut, and t cut (if any) that were used.

The topological-cross-section ratios σ_n/σ_T, where σ_n is the cross section for the reaction

$$\pi p \to n \text{ prongs}, \tag{8}$$

are presented in Table I. As can be seen, the agreement between on-shell and off-shell data is excellent.

In the following discussion, we compare distributions for on-shell and off-shell π^+p interactions. Comparison of on-shell and off-shell π^-p interactions gives essentially identical results.[13]

In Figs. 3 and 4, excellent agreement is seen between on-shell and off-shell invariant x distributions of

$$\frac{1}{\sigma_T}\frac{E^*}{p^*_{\max}}\frac{d\sigma}{dx},$$

where E^* and $p^*_{\max}$ are the center-of-mass values of energy and the maximum possible momentum, respectively (the "beam" direction for the off-shell data is defined as the opposite of the target proton direction in the X system rest frame). The distributions for the reaction

$$\pi^+p \to p + X \tag{9}$$

[Figs. 3(a) and 3(b)] have strong leading-proton peaks near $x = -1$ with the on-shell and off-shell distributions being indistinguishable. Furthermore, the peaks, both on-shell and off-shell, are found to be due entirely to the two-prong events [Figs. 3(c) and 3(d)] with events with more than two prongs having smoother distributions peaked near $x = -0.4$ [Figs. 3(e) and 3(f)]. Even broken down topologically, no significant differences are seen between on-shell and off-shell distributions. The effect of cuts in t (beam to ρ) upon the

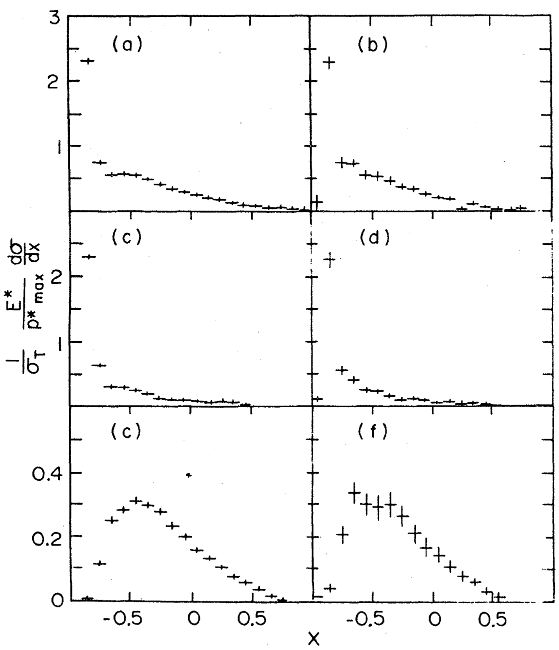

FIG. 3. (a) and (b) On-shell and off-shell invariant x distributions, respectively, for $\pi^+p \to p + X$. (c) and (d) Same as (a) and (b), but only two-prong events. (e) and (f) Same as (a) and (b), but only events with four or more prongs.

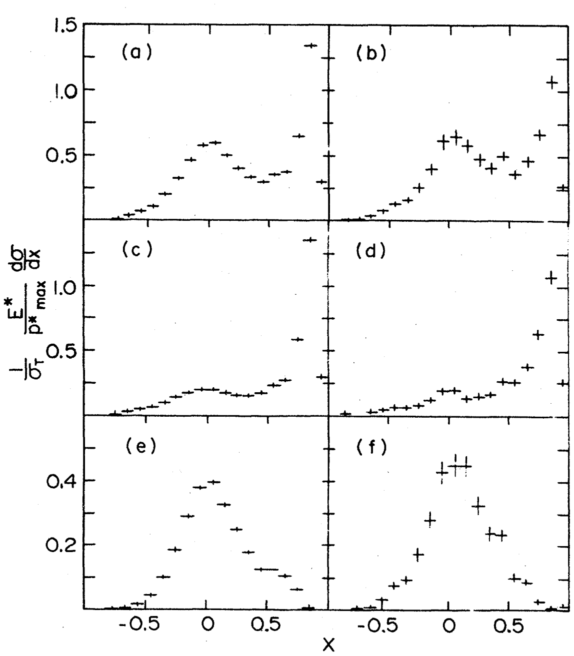

FIG. 4. (a) and (b) On-shell and off-shell invariant x distributions, respectively, for $\pi^+p \to \pi^+ + X$. (c) and (d) Same as (a) and (b), but only two-prong events. (e) and (f) Same as (a) and (b), but only events with four or more prongs.

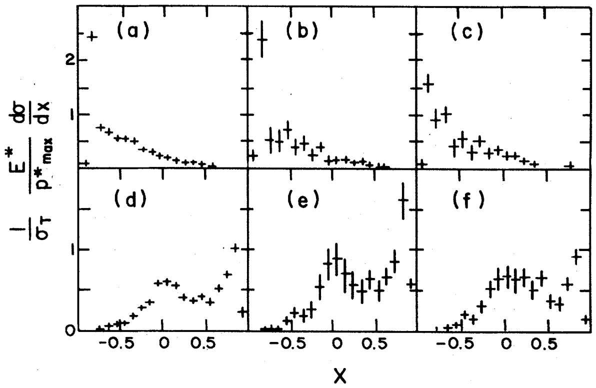

FIG. 5. (a) Off-shell $\pi^+p\to p+X$, invariant x distribution for $|t|<0.38$ GeV^2 (measured from beam to ρ). (b) Off-shell $\pi^+p\to p+X$, invariant x distribution for $0.38<|t|<0.74$ GeV^2. (c) Off-shell $\pi^+p\to p+X$, invariant x distribution for $|t|>0.74$ GeV^2. (d) Off-shell $\pi^+p\to\pi^++X$, invariant x distribution for $|t|<0.38$ GeV^2. (e) Off-shell $\pi^+p\to\pi^++X$, invariant x distribution for $0.38<|t|<0.74$ GeV^2. (f) Off-shell $\pi^+p\to\pi^++X$, invariant x distribution for $|t|>0.74$ GeV^2.

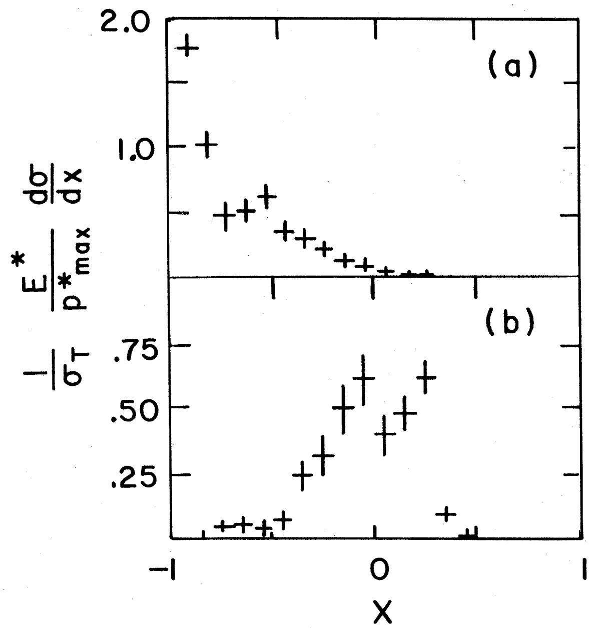

FIG. 6. (a) Invariant x distribution in the overall center of mass for the protons of Fig. 3(b). (b) Same as (a) for the π^+'s of Fig. 4(b).

invariant x distributions for reaction (9) can be seen in Figs. 5(a), 5(b), and 5(c). As t increases, the distributions broaden slightly and have less pronounced leading peaks, but the overall features remain the same.

The same distributions for the reaction

$$\pi^+p\to\pi^++X \tag{10}$$

[Figs. 4(a) and 4(b)] again show the remarkable similarity between on-shell and off-shell reactions. The distributions have a central peak near $x=0$ and, after a dip near $x=0.5$, a leading pion peak at $x\simeq0.9$. As with reaction (9), the leading peaks are seen to be entirely to the two-prong events [Figs. 4(c) and 4(d)], with the distributions for events in higher topologies [Figs. 4(e) and 4(f)] showing predominantly central production with a small forward excess near $x\simeq0.6$. The distributions for the reaction

$$\pi^+p\to\pi^-+X \tag{11}$$

(not shown) are similar to those for the higher topologies of reaction (10), showing the same forward excess. In all cases, the off-shell data repeat in detail the features seen in the on-shell distributions. Similarity is also seen in rapidity distributions (not shown). The invariant x distributions for reaction (10) for the three t cuts are shown in Figs. 5(d), 5(e), and 5(f). Once again, the distributions remain very similar as the mass of the off-shell pion increases.

It is also worth noting that the leading peaks in the off-shell data are not simply a reflection of similar peaks in the overall center of mass. Although the protons in the overall center of mass do show a strong peak near $x=-1$ [Fig. 6(a)], the peak due to pions, if any, is at $x=0.3$ [Fig. 6(b)], not near $x=1$. Of course, the x cut imposed on the ρ^0 limits the x values of the remaining pions, but there is no such peak near $x=0.3$ in the overall center of mass for the data containing no cut on x ($\pi^+\pi^-$).

We have also compared the p_T distribution of $(1/\sigma_T)d\sigma/dp_T^2$, where p_T is the transverse momentum of the outgoing particle. The distributions for reaction (9) [Figs. 7(a) and 7(b)] show similar slopes and structure for the on-shell and off-shell data. No clear break in the slope is found for $p_T^2 \lesssim 0.5$ (GeV/c)^2 for either data sample. In contrast, breaks in the slopes near $p_T^2\simeq0.2$ (GeV/c)^2 are seen for reactions (10) and (11), shown in Figs. 7(c)–7(f). To obtain a more quantitative comparison, fits of the form

$$\frac{1}{\sigma_T}\frac{d\sigma}{dp_T^2}=Ae^{-bp_T^2} \tag{12}$$

have been performed over various ranges in p_T^2 for all of these reactions. The results are shown as straight lines in Fig. 7 and are summarized in Table II. As before, the on-shell and off-shell

TABLE II. $d\sigma/dp_T^2$ slopes at 3.9 GeV/c. Results of fits to $d\sigma/dp_T^2 = Ae^{-bp_T^2}$.

Reaction		Range [(GeV/c)^2]	b [(GeV/c)$^{-2}$]
$\pi^- p \to p + X$	on-shell	0.00–0.35	6.18 ± 0.10
	off-shell	0.00–0.32	6.79 ± 0.80
$\pi^+ p \to p + X$	on-shell	0.00–0.50	5.40 ± 0.08
	off-shell	0.00–0.46	6.91 ± 2.15
$\pi^- p \to \pi^- + X$	on-shell	0.00–0.20	8.66 ± 0.10
	off-shell	0.00–0.20	9.84 ± 1.12
	on-shell	0.20–0.70	6.13 ± 0.09
	off-shell	0.20–0.68	5.96 ± 1.55
$\pi^+ p \to \pi^+ + X$	on-shell	0.00–0.20	10.26 ± 0.17
	off-shell	0.00–0.20	10.10 ± 0.75
	on-shell	0.20–0.70	5.94 ± 0.11
	off-shell	0.20–0.68	6.09 ± 1.10
$\pi^- p \to \pi^+ + X$	on-shell	0.00–0.20	11.48 ± 0.13
	off-shell	0.00–0.20	12.41 ± 2.08
	on-shell	0.20–0.70	6.55 ± 0.13
	off-shell	0.20–0.68	3.85 ± 2.60
$\pi^+ p \to \pi^- + X$	on-shell	0.00–0.20	11.82 ± 0.25
	off-shell	0.00–0.20	10.67 ± 2.52
	on-shell	0.20–0.70	8.46 ± 0.19
	off-shell	0.20–0.68	9.84 ± 2.10

distributions are found to be in generally excellent agreement. No systematic effect on the slopes due to cuts in the off-shell pion mass has been found.

As a final comparison, we have also examined the t distributions of $d\sigma/dt$ for elastic scattering, where t here is defined as the four-momentum transfer between the target proton and final-state proton. Off-shell elastic-scattering events are those of the overall final state $p\rho^0\pi^\pm$, which have been studied separately. In this data sample, the amount of background under the ρ^0 is so small that background subtraction has not been performed. The distributions of $(1/\sigma_T)d\sigma/dt$ for the off-shell data are shown in Fig. 8. Fits of the form

$$\frac{1}{\sigma_T}\frac{d\sigma}{d|t|} = Ae^{-b|t|} \tag{13}$$

have been performed over the ranges $0.1 < |t| < 0.4$ (GeV/c)^2 for the $\pi^+ p$ data and $0.025 < |t| < 0.5$ (GeV/c)^2 for the $\pi^- p$ data, with the results shown as straight lines in Fig. 8. The off-shell $\pi^+ p$ slope $b = 6.51 \pm 0.14$ (GeV/c)$^{-2}$ is indistinguishable from the on-shell result[14] of $b = 6.61 \pm 0.56$ (GeV/c)$^{-2}$, and the off-shell $\pi^- p$ result $b = 7.66 \pm 0.40$ (GeV/c)$^{-2}$ is also in excellent agreement with the on-shell

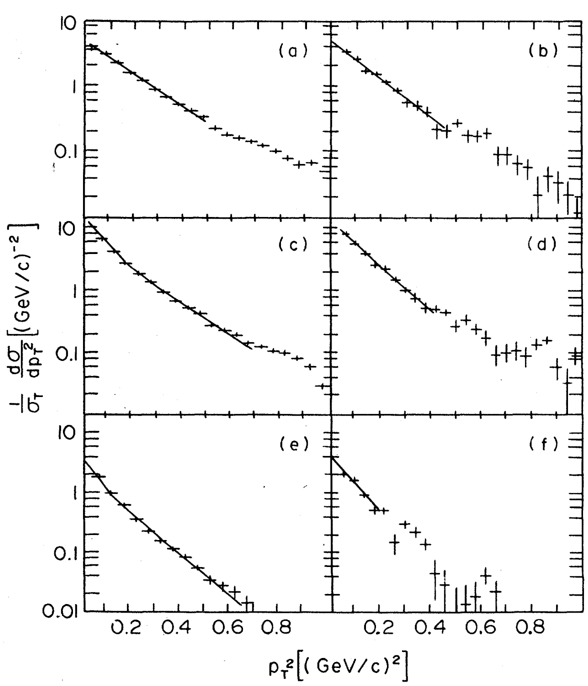

FIG. 7. (a) and (b) On-shell and off-shell p_T^2 distributions, respectively, for $\pi^+ p \to p + X$. (c) and (d) Same as (a) and (b) for $\pi^+ p \to \pi^+ + X$. (e) and (f) Same as (a) and (b) for $\pi^+ p \to \pi^- + X$. The straight lines are the results of fits; see text and Table II.

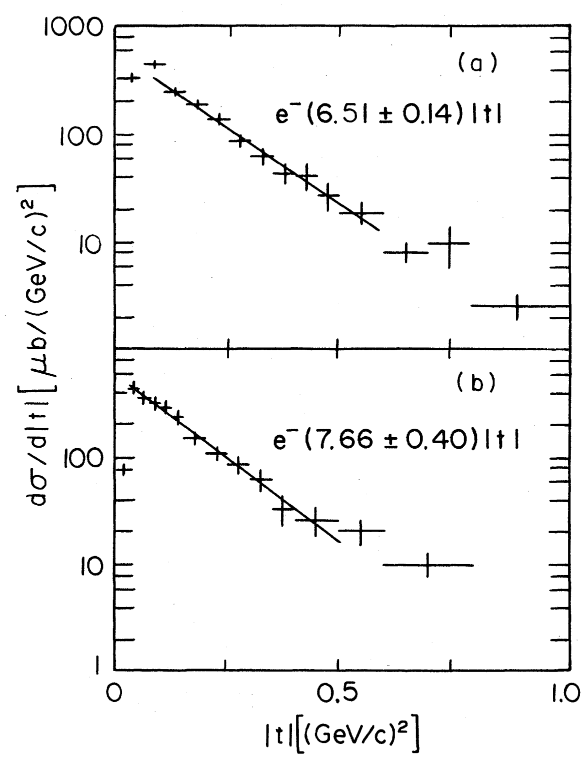

FIG. 8. (a) Off-shell t distributions for $\pi^+ p \to \pi^+ p$. (b) Same as (a) for $\pi^- p \to \pi^- p$. The straight lines are the results of fits; see text.

value[15] of $b = 7.92 \pm 0.72$ $(\text{GeV}/c)^{-2}$.

The remarkable similarity of all of these distributions leads us to conclude that off-shell pions do in fact behave like on-shell pions. It is also worth noting that if one assumes that on-shell and off-shell pions should behave similarly, then the evidence presented here strongly suggests that pion exchange is truly the dominant ρ^0 production mechanism in the region studied.

IV. INCLUSIVE Δ^{++} PRODUCTION AND OFF-SHELL $\pi\pi$ INTERACTIONS

In the previous section, we have shown that off-shell pions interact with protons in the same way as real pions. In this section, we present a study of the interactions of off-shell pions with real pions, using pion exchange in the reactions

$$\pi^+ p \to \Delta^{++} + X^0 \tag{14}$$

and

$$\pi^- p \to \Delta^{++} + X^{--} \tag{15}$$

as the off-shell pion source. The upper vertices of these reactions, as diagrammed in Fig. 9(a), may then be viewed as the reactions

$$\pi^+\pi^- \to X^0 \tag{16}$$

and

$$\pi^-\pi^- \to X^{--}. \tag{17}$$

For this part of the analysis, only events with identified protons have been considered. To identify a sample of events dominated by pion exchange, we have studied the spin-density-matrix element ρ_{33} as a function of t (measured from the target proton to the Δ^{++}). For pure one-pion exchange, ρ_{33} is predicted to have the value $\rho_{33} = 0$, while for pion exchange with absorption, its predicted value[16] is $\rho_{33} = 0.12$. A method of moments calculation, in which

$$\rho_{33} = (7 - 15\langle\cos^2\theta_J\rangle)/8\,, \tag{18}$$

where θ_J is the t-channel Gottfried-Jackson decay angle of the Δ^{++}, has been performed in various t intervals. In order to obtain a reasonably pure Δ^{++} sample, only events with $1120 < M(p\pi^+) < 1360$ MeV and $\cos\theta_J < 0$ have been used for this calculation. (The background has been found to have distributions sharply peaked near $\cos\theta_J = 1$, with virtually all events in the forward hemisphere.) The results indicate that ρ_{33} has a value consistent with $\rho_{33} = 0.12$ for $|t| < 0.4$ $(\text{GeV}/c)^2$ in the $\pi^- p$ data ($\rho_{33} = 0.14 \pm 0.02$), while in the $\pi^+ p$ data, a more limited cut of $|t| < 0.3$ $(\text{GeV}/c)^2$ has been used, leaving a sample of events with $\rho_{33} = 0.130 \pm 0.006$. Making these t cuts also leaves us with very little

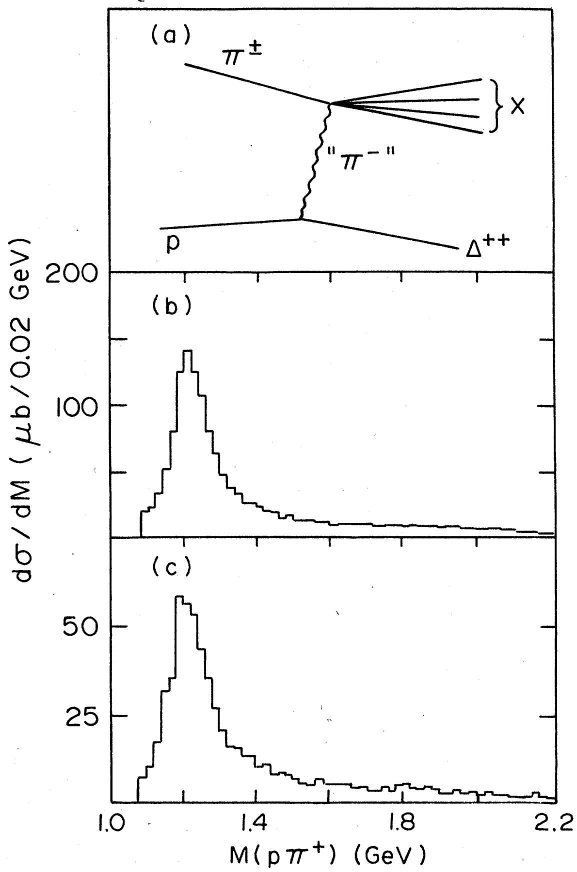

FIG. 9. (a) Feynman diagram for inclusive Δ^{++} production by pion exchange. (b) $p\pi^+$ effective-mass distribution for $\pi^+ p \to \Delta^{++} + X$ with $t_{p\Delta} < 0.3$ $(\text{GeV}/c)^2$. (c) Same as (b) for $\pi^- p \to \Delta^{++} + X$ with $t_{p\Delta} < 0.4$ $(\text{GeV}/c)^2$.

background. The $p\pi^+$ effective-mass distributions for events in these t cuts [Figs. 9(b) and 9(c)] have been fit to the sum of a Breit-Wigner mass shape and a polynomial background. The amount of background thus found in the mass cut used to define the Δ^{++} $[1120 < M(p\pi^+) < 1360$ MeV$]$ is only 16% for the $\pi^+ p$ data sample and 22% for the $\pi^- p$ data sample. Since these percentages are so small, no background subtraction has been performed. Note also that this t cut should eliminate even the small effects noted in the previous section due to massive pions.

As a consistency check, we have also performed a triple-Regge analysis of reaction (15). Assuming Pomeron dominance at the exotic vertex, and with an assumed Pomeron intercept of $\alpha_P(0) = 1$, the effective trajectory of the exchanged particle has been found to be consistent with the expected pion trajectory for $|t| \lesssim 0.4$ $(\text{GeV}/c)^2$, while at higher values of $|t|$, the effective trajectory has been found to approach the trajectory expected for the ρ. In general, these results are the same as those found in an earlier study[4] which was not limited to identified protons.

Although pion exchange dominates in the t cuts used, there is a class of events that cannot be due to pion exchange, such as the final state $\Delta^{++}\pi^0$. In order to conserve G parity in pion-exchange reactions, one needs at least two pions at the upper vertex in Fig. 9(a). The few events with $M_X < 279$ MeV (where M_X is the mass of the system recoiling against the Δ^{++}) have therefore been eliminated from the sample. The Δ^{++} mass cut then leaves us with 925 μb (19 032 events) in the π^+p data sample and 410 μb (2463 events) in the π^+p data sample.

The M_X^2 distributions for these events are shown in Fig. 10. As expected for an exotic system, the π^-p data distribution [Fig. 10(b)] shows no significant structure. In the π^+p data [Fig. 10(a)], however, if one looks at values of M_X^2 corresponding to the ρ^0 ($M_X^2 \simeq 0.6$ GeV^2), the f^0 ($M_X^2 \simeq 1.6$ GeV^2), and the g^0 ($M_X^2 \simeq 2.7$ GeV^2) resonances, one sees indications of small peaks. At these M_X^2 values, s-channel resonance formation might be expected to dominate reaction (16). It therefore seems appropriate to study these regions of M_X^2 separately. To this end, the $\pi^+\pi^-$ data sample has been studied in five separate M_X^2 intervals:

$$M_X^2 < 1.25 \text{ GeV}^2,$$

$$1.25 < M_X^2 < 2.50 \text{ GeV}^2,$$

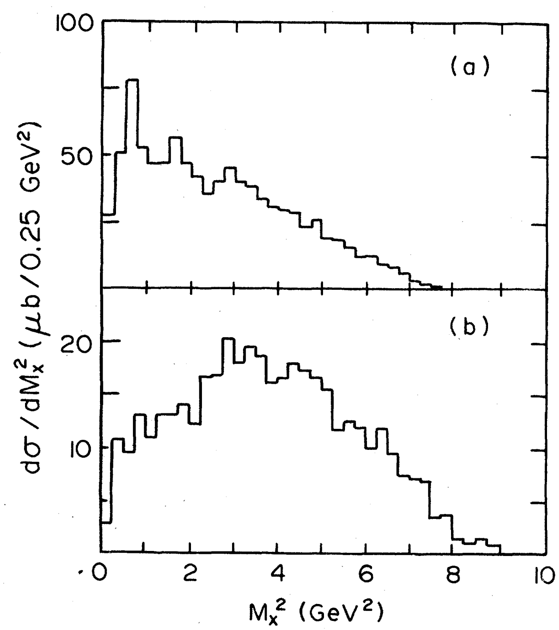

FIG. 10. (a) M_X^2 distribution for $\pi^+p \to \Delta^{++} + X$ with $t_{p\Delta} < 0.3$ (GeV/c)^2. (b) Same as (a) for $\pi^-p \to \Delta^{++} + X$ with $t_{p\Delta} < 0.4$ (GeV/c)^2.

$$2.50 < M_X^2 < 3.75 \text{ GeV}^2, \quad 3.75 < M_X^2 < 5.00 \text{ GeV}^2, \tag{19}$$

and

$$M_X^2 > 5.00 \text{ GeV}^2.$$

Since M_X^2 corresponds to s for $\pi\pi$ interactions, the energy dependence may also be studied in this way. Similarly, we have divided the $\pi^-\pi^-$ data into four different M_X^2 intervals:

$$M_X^2 < 2.5 \text{ GeV}^2, \quad 2.5 < M_X^2 < 4.0 \text{ GeV}^2, \quad 4.0 < M_X^2 < 5.5 \text{ GeV}^2, \tag{20}$$

and

$$M_X^2 > 5.5 \text{ GeV}^2.$$

These divisions were chosen to provide each interval with roughly the same number of events, as there are no resonances to provide natural M_X^2 regions.

As with the off-shell πp data of the previous section, we have not calculated absolute total $\pi\pi$ cross sections but have instead normalized all distributions by dividing by σ_T, which is the total cross section in a given M_X^2 interval for Δ^{++} production as defined above. The ratios σ_{el}/σ_T, where σ_{el} is the cross section for $\pi\pi$ elastic scattering (i.e., the events of the overall final state $\Delta^{++}\pi^{\pm}\pi^-$), and σ_n/σ_T, where σ_n is the cross section for

$$\pi\pi \to n \text{ charged prongs}, \tag{21}$$

are presented in Table III. The sharp drop in σ_{el}/σ_T with increasing energy is in good general agreement with the results of a one-pion-exchange-model study[10] of π^-p data at 25 GeV/c. The ratio σ_{el}/σ_T is also seen to be higher for $\pi^-\pi^-$ interactions than for $\pi^+\pi^-$ interactions as a function of M_X^2 over the entire M_X^2 range (Fig. 11). A naive explanation of this phenomenon may be that the absence of any zero-prong channels and the exotic nature of one of the vertices in any charge-exchange reaction suppress the inelastic part of the $\pi^-\pi^-$ cross section relative to that for $\pi^+\pi^-$ interactions. Similar effects are seen in the differences in σ_{el}/σ_T between pp and $\bar{p}p$,[17] π^+p and π^-p,[18] and K^+p and K^-p (Ref. 19) interactions, where for a given value of s (for $s \lesssim 10$ GeV^2), σ_{el}/σ_T is greater for the states with net charge $Q = 2$ than for those with $Q = 0$.

The average charged-particle multiplicities $\langle n_X \rangle$ for $\pi^+\pi^-$ and $\pi^-\pi^-$ interactions are presented in Table IV and plotted in Fig. 12. Several theoretical models have been introduced to describe the energy dependence of $\langle n_X \rangle$; they are discussed in works by Frazer *et al.*[20] and by Brick *et al.*[21] In an effort to compare the predictions of these

TABLE III. Topological-cross-section ratios σ_n/σ_T in $\pi\pi$ interactions.

Prongs \ M_X^2 range (GeV^2)	0.0–2.5	2.5–4.0	4.0–5.5	5.5–max	
	$\pi^-\pi^- \to n$ prongs				
2	0.963 ± 0.008	0.815 ± 0.016	0.723 ± 0.019	0.579 ± 0.022	
2 (elastic)	0.677 ± 0.017	0.336 ± 0.018	0.238 ± 0.018	0.126 ± 0.022	
4	0.033 ± 0.007	0.176 ± 0.016	0.269 ± 0.019	0.343 ± 0.021	
6	0.004 ± 0.003	0.009 ± 0.004	0.008 ± 0.004	0.071 ± 0.013	
8				0.007 ± 0.005	
	$\pi^+\pi^- \to n$ prongs				
Prongs \ M_X^2 range (GeV^2)	0.00–1.25	1.25–2.50	2.50–3.75	3.75–5.00	5.00–max
0	0.216 ± 0.007	0.209 ± 0.008	0.086 ± 0.005	0.086 ± 0.006	0.065 ± 0.007
2	0.777 ± 0.008	0.737 ± 0.009	0.705 ± 0.012	0.595 ± 0.015	0.521 ± 0.020
2 (elastic)	0.602 ± 0.011	0.324 ± 0.011	0.163 ± 0.010	0.114 ± 0.010	0.055 ± 0.008
4	0.007 ± 0.002	0.053 ± 0.006	0.201 ± 0.011	0.296 ± 0.015	0.372 ± 0.019
6	0.0004 ± 0.0002	0.0009 ± 0.0004	0.008 ± 0.003	0.023 ± 0.007	0.042 ± 0.010
8	0.0002 ± 0.0002	0.0003 ± 0.0003			0.0005 ± 0.0005

models with experimentally observed multiplicities, Albini *et al.*[22] have compiled an extensive list of experimental results for numerous on-shell reactions and performed fits using various formulas. The limited accuracy of the data and the limited energy range over which experimental results are available have been found to make discrimination between models difficult. Nonetheless, Albini *et al.*[22] observe that if an appropriate energy variable is used, multiplicities from all different reactions tend to follow a "universal curve."

However, Brick *et al.*[21] and the Proportional Hybrid System Consortium[23] note that this universality is only approximate. They observe small but significant differences in $\langle n_X\rangle$ as a function of the incident-particle types, which Brick *et al.*[21] explain in terms of a simple model. As diagrammed in Fig. 12, $\langle n_X\rangle$ is made up of contributions from three sources. The incoming particles, a and b, contribute n_a and n_b, respectively, which depend only on particle type. There is also a contribution from the central region which is proportional to $\ln s$. Thus, the average charged-particle multiplicity can be written as

$$\langle n_X\rangle = n_a + B\ln s + n_b\,, \qquad (22)$$

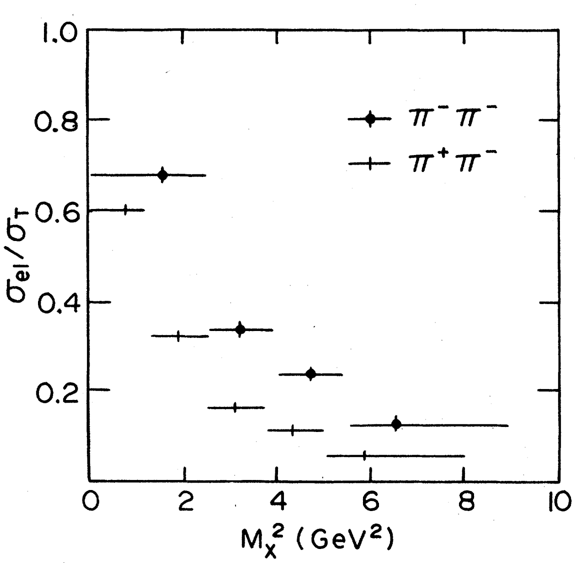

FIG. 11. σ_{el}/σ_T vs M_X^2 for $\pi^+\pi^-$ and $\pi^-\pi^-$ interactions.

TABLE IV. Average charged-particle multiplicities $\langle n_X\rangle$ in inelastic $\pi\pi$ interactions.

M_X^2 range (GeV^2)	Weighted average value of M_X^2 (GeV^2)	$\langle n_X\rangle$
	$\pi^-\pi^-$	
0.0–2.5	1.62	2.258 ± 0.054
2.5–4.0	3.23	2.584 ± 0.049
4.0–5.5	4.70	2.746 ± 0.056
5.5–max	6.57	3.157 ± 0.070
	$\pi^+\pi^-$	
0.00–1.25	0.819	0.959 ± 0.036
1.25–2.50	1.88	1.543 ± 0.030
2.50–3.75	3.10	2.315 ± 0.034
3.75–5.00	4.33	2.580 ± 0.046
5.00–max	5.86	2.832 ± 0.056

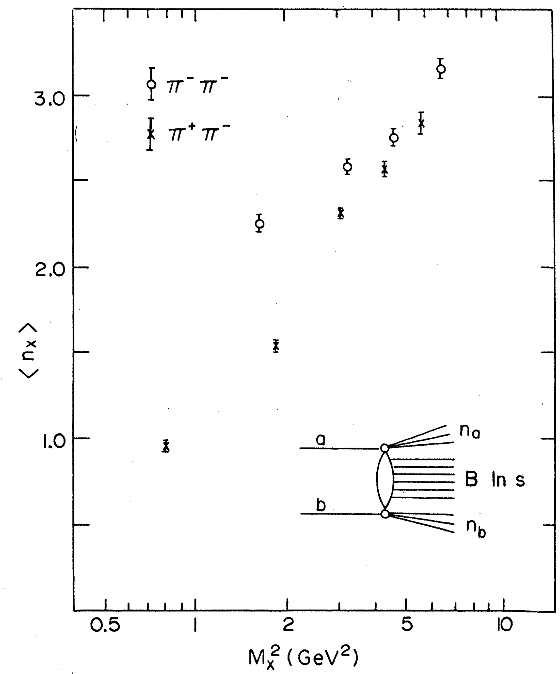

FIG. 12. Average multiplicity vs M_X^2 for $\pi\pi$ interactions. Diagram corresponds to simple model discussed in text.

where B is a universal constant.

To compare the $\pi\pi$ multiplicites with those of other reactions, fits have been performed to the data in Fig. 12 and data from the compilation of Albini *et al.*[22] Each reaction has been fit separately. In the case of the $\pi\pi$ data, the weighted average value of M_X^2 in each M_X^2 interval (see Table IV) has been used in place of s. Unfortunately, these values of M_X^2 are small by comparison with available values of s for on-shell reactions; the largest value of M_X^2 for either $\pi^+\pi^-$ or $\pi^-\pi^-$ reactions is smaller than the smallest value of s for any on-shell reaction. To make comparison even more difficult, these M_X^2 values are also in a region in which threshold effects may be important. We have therefore limited the on-shell data used to the region $s < 30$ GeV^2 (using only $s < 20$ GeV^2 gives the same results). We have also used a minimum error of 1% of the average multiplicity on each point to compensate for different systematic errors in the on-shell data, which come from may different experiments. Finally, we have fit the data to the form

$$\langle n_X \rangle = A + B \ln(s/s_0)\,, \tag{23}$$

where $s_0 = 8$ GeV^2. The differences between the values of A for different reactions are then the differences in $\langle n_X \rangle$ in the region where on-shell and off-shell energies are most similar.

The results of these fits are presented in Table V. As predicted by the model, the parameter B is seen to have a universal value of $B \simeq 1.0$, with the exception of the $\pi^-\pi^-$ value of $B \simeq 0.6$. However, $\pi^-\pi^-$ reactions are something of a special case. Because of the very low energy range of this study, threshold effects in $\pi^-\pi^-$ reactions are extremely important. As seen in Fig. 12, the lowest energy $\pi^-\pi^-$ points come very close to the minimum possible multiplicity (there must be at least two charged particles). At larger values of M_X^2, however, the points for $\pi^-\pi^-$ interactions are found to lie near those for $\pi^+\pi^-$ interactions, and it appears likely that the $\pi^-\pi^-$ slope is getting steeper as M_X^2 leaves the threshold region.

The values of the parameter A indicate that the $\pi^+\pi^-$ and $\pi^-\pi^-$ multiplicites are essentially equal (for energies well above threshold) and higher than for other reactions at a given energy. Comparison of A in the context of Eq. (22) gives the result

$$n_{\pi^+} - n_{\pi^-} = 0.02 \pm 0.07\,. \tag{24}$$

This result is consistent with the value zero predicted by the model considers the three contributions to $\langle n_X \rangle$ to be completely independent, charge-conjugation invariance demands that

$$n_{\pi^+} = n_{\pi^-}\,. \tag{25}$$

We note, however, that comparison of A for π^+p and π^-p reactions gives a different result:

$$n_{\pi^+} - n_{\pi^-} = 0.47 \pm 0.06\,. \tag{26}$$

This difference may be attributed to two factors. First, resonant final states (such as $\Delta^{++}\rho^0$) are not considered by the model, although resonance production is known to contribute a large part of the cross section in the relatively low energy range studied here. Thus, any difference between resonance production in π^+p and π^-p interactions could affect the results. Second, there may be threshold effects, especially in π^+p interactions where there must be at least two charged particles. Significantly, at higher energies π^+p and π^-p interactions give comparable multiplicities; Brick *et al.*[21] use π^+p and π^-p reactions to find

$$n_{\pi^+} - n_{\pi^-} = 0.09 \pm 0.03\,, \tag{27}$$

which is consistent with Eq. (24). Because of the threshold effects, we consider the π^-p multiplicity to have more validity in terms of the model than the π^+p multiplicity.

We can then use the values of A for $\pi^+\pi^-$ and π^-p reactions to obtain the result

$$n_{\pi^+} - n_p = 0.59 \pm 0.07\,, \tag{28}$$

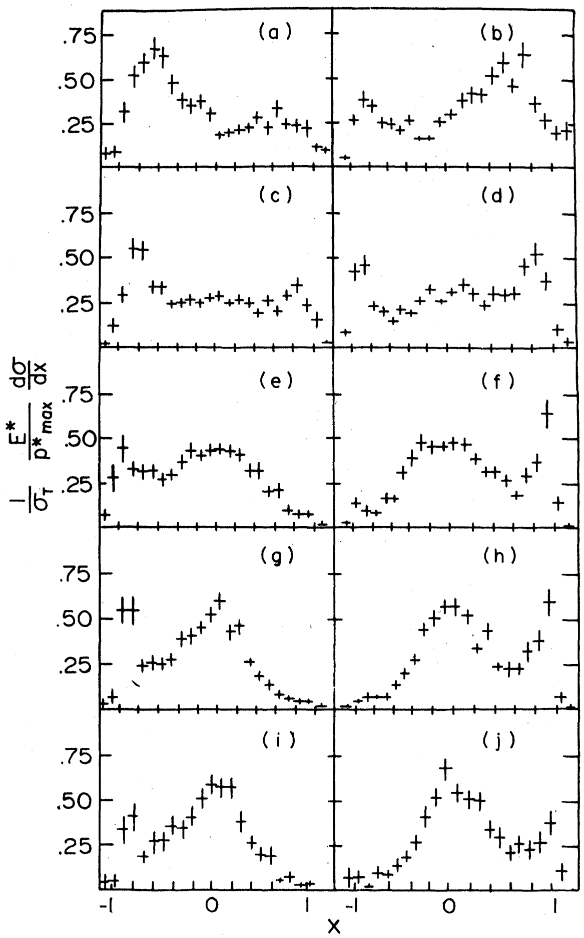

FIG. 13. (a) and (b) Invariant x distributions for $\pi^+\pi^- \to \pi^+ + X'$ and $\pi^+\pi^- \to \pi^- + X$, respectively, for $M_X{}^2 < 1.25$ GeV^2. (c) and (d) Same as (a) and (b) for $1.25 < M_X{}^2 < 2.50$ GeV^2. (e) and (f) Same as (a) and (b) for $2.50 < M_X{}^2 < 3.75$ GeV^2. (g) and (h) Same as (a) and (b) for $3.75 < M_X{}^2 < 5.00$ GeV^2. (i) and (j) Same as (a) and (b) for $M_X{}^2 > 5.00$ GeV^2.

while the values of A for $\pi^-\pi^-$ and π^-p reactions gives

$$n_{\pi^-} - n_p = 0.57 \pm 0.08\,. \tag{29}$$

These results are also in excellent agreement with those obtained at higher energies by Brick *et al.*[21]:

$$n_{\pi^+} - n_p = 0.64 \pm 0.03 \tag{30}$$

and

$$n_{\pi^-} - n_p = 0.55 \pm 0.03\,. \tag{31}$$

The observed universality of the parameter B and the agreement with other results suggest that with the exceptions already noted, the model works rather well, even at these low energies. This result is actually somewhat surprising since at these energies, there is really no central region. In particular, the formation of ρ^0 and f^0 mesons in s-channel $\pi^+\pi^-$ reactions is not at all consistent with the model's concept of independent vertices as diagrammed in Fig. 12. The fact that the parametrization of the model does work so well, in spite of the model's acknowledged limitations, may be indicative of some more general aspect of hadron production than that which the model considers.

The invariant distributions in x of

$$\frac{1}{\sigma_T}\,\frac{E^*}{p^*_{\max}}\,\frac{d\sigma}{dx}$$

for the reactions

$$\pi^+\pi^- \to \pi^+ + X' \tag{32}$$

and

$$\pi^+\pi^- \to \pi^- + X' \tag{33}$$

in the different $M_X{}^2$ intervals are shown in Fig. 13. Since the $\pi^+\pi^-$ system is its own charge conjugate, the longitudinal-momentum distributions for reactions (32) and (33) should be mirror images of each other. Such symmetry is indeed observed. The leading-particle peaks near $x = 1$ for π^- production and near $x = -1$ for π^+ production have been found to be made up almost exclusively of the elastic events

$$\pi^+\pi^- \to \pi^+\pi^-\,. \tag{34}$$

The small "backward" peaks (near $x = 1$ for π^+ production and $x = -1$ for π^-p production) seen in the intervals with smaller $M_X{}^2$ are due to the backward decay ($\cos\theta_J \simeq -1$) of the ρ^0 and f^0 mesons which are produced in the s channel and have decay angular distributions peaked at $\cos\theta_J \simeq \pm 1$.

The same distributions for the reaction

$$\pi^-\pi^- \to \pi^- + X' \tag{35}$$

are presented in Fig. 14. As expected, the distributions are symmetric about $x = 0$. The leading peaks near $x = \pm 1$ have again been found to be due to the elastic events

$$\pi^-\pi^- \to \pi^-\pi^- \tag{36}$$

in all $M_X{}^2$ intervals. The distributions for the reaction

$$\pi^-\pi^- \to \pi^+ + X' \tag{37}$$

(Fig. 15) therefore show no leading peaks but are very similar to the distributions for the higher topologies (≥ 4 prongs) of reactions (32), (33), and (35) (not shown).

As indicated in the previous section, these off-

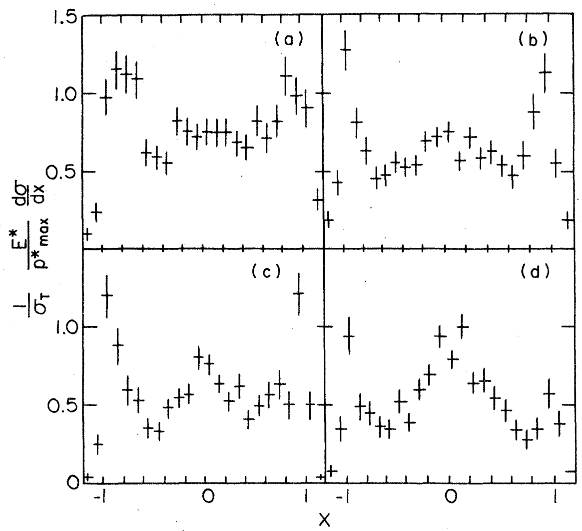

FIG. 14. Invariant x distributions for $\pi^-\pi^- \to \pi^- + X'$ for (a) $M_X^2 < 2.5$ GeV^2, (b) $2.5 < M_X^2 < 4.0$ GeV^2, (c) $4.0 < M_X^2 < 5.5$ GeV^2, (d) $M_X^2 > 5.5$ GeV^2.

shell leading peaks are not simply a reflection of leading peaks in the overall center of mass. The invariant x distributions in the overall center-of-mass system for the pions of Figs. 13(g) and 13(h) (a representative sample) are shown in Fig. 16. Although the π^+ peak is seen to be part of a real leading peak ($x \simeq 0.9$), the π^- distribution shows only a broad distribution peaking at $x \simeq 0.2$.

The lack of any leading-particle peaks in the higher topologies agrees well with the results of a recent study[9] of the reaction

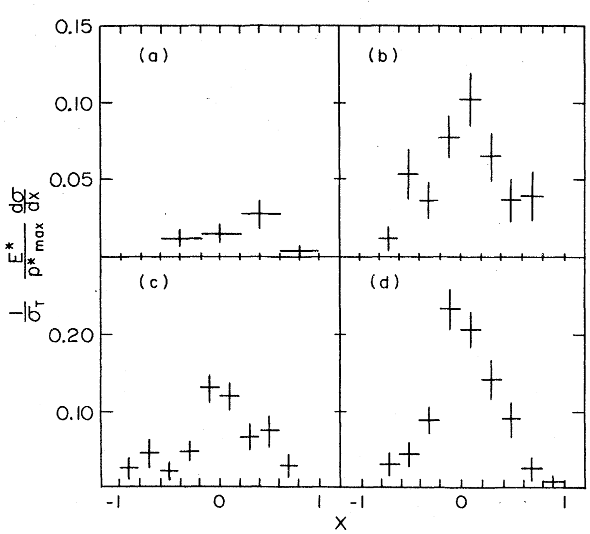

FIG. 15. Invariant x distributions for $\pi^-\pi^- \to \pi^+ + X'$ for (a) $M_X^2 < 2.5$ GeV^2, (b) $2.5 < M_X^2 < 4.0$ GeV^2, (c) $4.0 < M_X^2 < 5.5$ GeV^2, (d) $M_X^2 > 5.5$ GeV^2.

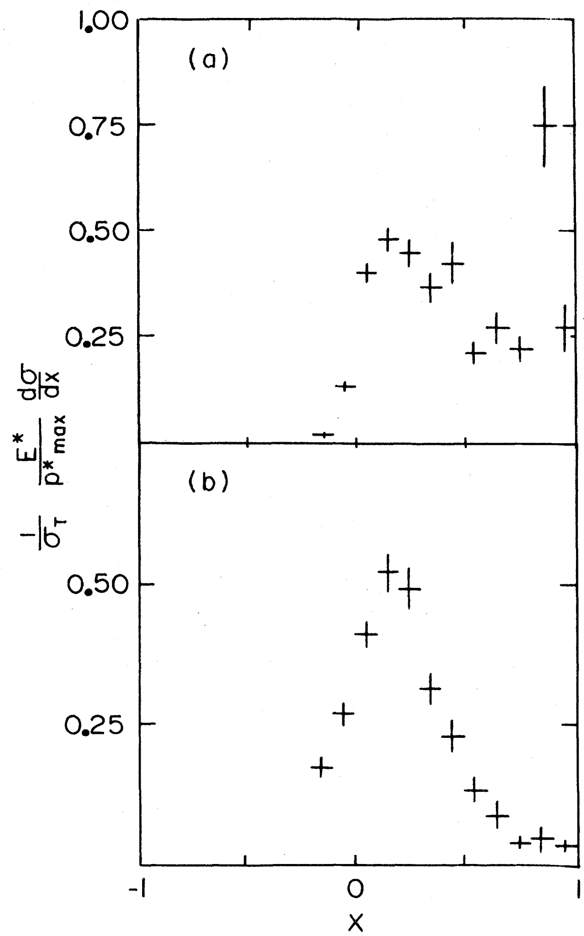

FIG. 16. (a) and (b) Invariant x distributions in the overall center of mass for the pions of Figs. 18(g) and 18(h), respectively.

$$\pi^- p \to \pi^-\pi^-\pi^+\pi^+ X^0 \tag{38}$$

(where X^0 contains only neutrals) at 147 GeV/c. Some events of this reaction have been interpreted as the off-shell reaction

$$``\pi^{+}"\pi^- \to \pi^+\pi^+\pi^-\pi^- . \tag{39}$$

Similar x distributions with no leading peaks were found for events with $s < 9$ GeV^2 (where $\sqrt{s}$ here represents the energy of the four-pion system), although at larger values of s leading peaks have been seen, corresponding to $A^\pm$ meson production.

The transverse-momentum distributions of $(1/\sigma_T)d\sigma/dp_T^2$ for reactions (32), (33), and (35) are shown in Figs. 17–19. With the exception of the two lowest-energy intervals of reactions (32) and (33), all distributions have exponential slopes that change at $p_T^2 \simeq 0.25$ (GeV/c)^2. We have performed fits to Eq. (12) for various ranges of p_T^2; the re-

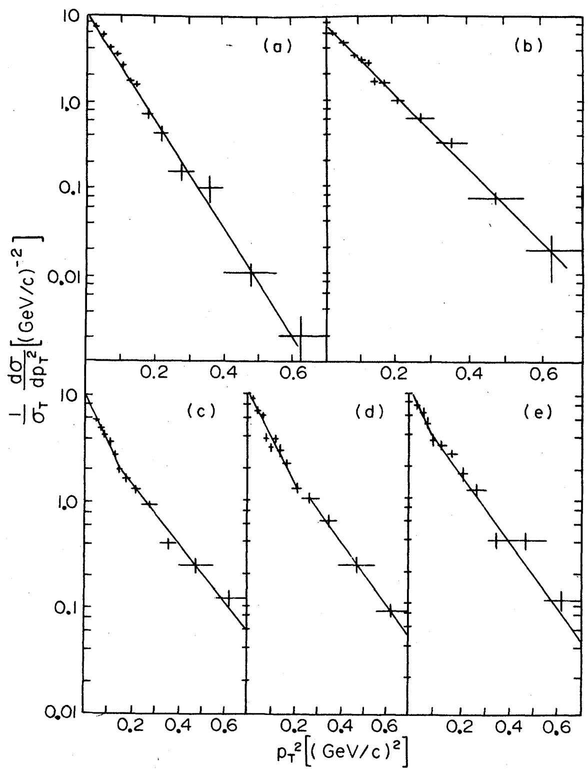

FIG. 17. p_T^2 distributions for $\pi^+\pi^- \to \pi^+ + X'$ for (a) $M_X^2 < 1.25$ GeV^2, (b) $1.25 < M_X^2 < 2.50$ GeV^2, (c) $2.50 < M_X^2 < 3.75$ GeV^2, (d) $3.75 < M_X^2 < 5.00$ GeV^2, (e) $M_X^2 > 5.00$ GeV^2. The straight lines are the results of fits; see text and Table VI.

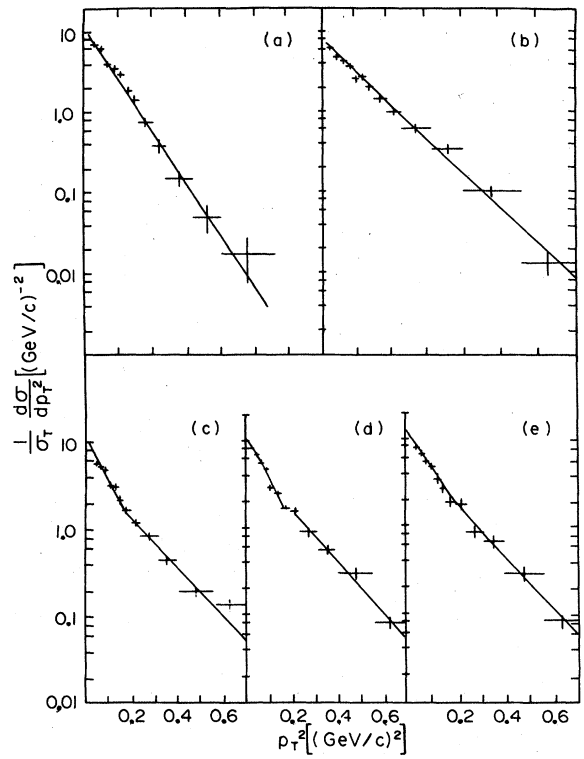

FIG. 18. p_T^2 distributions for $\pi^+\pi^- \to \pi^- + X'$ for (a) $M_X^2 < 1.25$ GeV^2, (b) $1.25 < M_X^2 < 2.50$ GeV^2, (c) $2.50 < M_X^2 < 3.75$ GeV^2, (d) $3.75 < M_X^2 < 5.00$ GeV^2, (e) $M_X^2 > 5.00$ GeV^2. The straight lines are the results of fits; see text and Table VI.

sults are shown as straight lines in Figs. 17–19 and summarized in Table VI. The slopes for reactions (32) and (33) are seen to be the same, withing the uncertainties, in each M_X^2 interval.

The break in the p_T^2 slopes has been explained[24] as resulting from two types of processes common to all interactions. The steep part of the slope is attributed to pions which are the decay products of resonances, while the shallow part is due to direct pion production. (If resonances are themselves produced with limited transverse momentum, their decay products, which must share this momentum, will have on the average even smaller p_T^2.) The absence of a break in slope in the first two M_X^2 intervals for reactions (32) and (33) indicates that these regions are dominated by ρ^0 and f^0 production. Indeed, the slopes in these M_X^2 intervals are comparable to the steep parts of the slopes in other M_X^2 intervals. However, even in the shallow slope regions, the values of the parameter b in Eq. (12) (see Table VI) are found to be generally greater than 5.0 $(\text{GeV}/c)^{-2}$, in contrast to a reported[24] universal slope of about 3.4 $(\text{GeV}/c)^{-2}$. It would be interesting to study higher-p_T^2 regions than the statistics here permit, in order to see if the slopes become even shallower.

Further evidence that the lowest M_X^2 intervals of reactions (32) and (33) are dominated by resonance production is provided by the $\pi^+\pi^-$ effective-mass distributions for pions produced in the reaction

$$\pi^+\pi^- \to \pi^+\pi^- + X' \tag{40}$$

(where X' may be nothing), shown in Fig. 20. For $M_X^2 < 1.25$ GeV^2, the majority of the outgoing pions are indeed seen to be ρ^0 decay products. For $1.25 < M_X^2 < 2.50$ GeV^2, a large shoulder at the ρ^0 mass as well as a large, clear peak at the f^0 mass again make up the bulk of the cross section. Clear ρ^0 and g^0 peaks are seen in the interval $2.50 < M_X^2 < 3.75$ GeV^2, but they no longer contain the vast majority of events. For $M_X^2 > 3.75$ GeV^2, small peaks at the ρ^0 mass are still seen, but their contribution to the cross section is relatively insignificant.

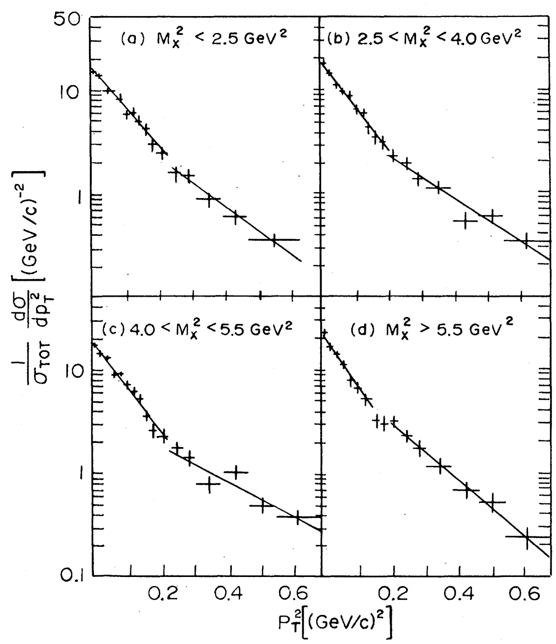

FIG. 19. p_T^2 distributions for $\pi^-\pi^- \to \pi^- + X'$ for (a) $M_X^2 < 2.5$ GeV^2, (b) $2.5 < M_X^2 < 4.0$ GeV^2, (c) $4.0 < M_X^2 < 5.5$ GeV^2, (d) $M_X^2 > 5.5$ GeV^2. The straight lines are the results of fits; see text and Table V.

In contrast, the $\pi^+\pi^-$ effective-mass distributions for the reaction

$$\pi^-\pi^- \to \pi^+\pi^- + X' \tag{41}$$

(Fig. 21) show no large resonant peaks, although evidence of ρ^0 production is found in all M_X^2 intervals.

Finally, the $|t|$ distributions of $(1/\sigma_T)d\sigma/d|t|$ for $\pi^+\pi^-$ and $\pi^-\pi^-$ elastic scattering are presented in Figs. 22 and 23. Unfortunately, the statistical uncertainties require plotting the data in relatively coarse bins, particularly at large values of M_X^2, where the ratio σ_{el}/σ_T has been found to be quite small (see Table III). The rise in $d\sigma/d|t|$ at large values of $|t|$ for $1.25 < M_X^2 < 3.75$ GeV^2 in the $\pi^+\pi^-$ data is attributed to the backward decay of the f^0 and the g^0. Fits of the form of Eq. (13) have been performed, but the results are found to be highly sensitive to the $|t|$ range used. Therefore, instead of plotting the results, we have summarized them in Table VII. Despite the large uncertainties, it is evident that the slope for $\pi^-\pi^-$ interactions gets steeper with increasing energy, although such shrinkage of the diffraction peak is not apparent in the $\pi^+\pi^-$ results. In general, the values of the slopes for both $\pi^+\pi^-$ and $\pi^-\pi^-$ interactions are also comparable to the value $b = 6$ (GeV/c)$^{-2}$ found in another study[10] and predicted by a quark-model calculations.[25] However, we know of no other study that has examined the energy dependence of the slope in such interactions.

V. SUMMARY AND CONCLUSIONS

We have used pion exchange in reactions (1)–(4) at 15 GeV/c to study off-shell $\pi^{\pm}p$ and $\pi^{\pm}\pi^-$ interactions. Comparison of on-shell and off-shell $\pi^{\pm}p$ interactions reveals no discernible differences, leading to the conclusion that off-shell pions do in fact behave like real pions. Off-shell pions with large negative mass squared show only small differences in behavior from lighter off-shell pions.

The off-shell reactions (16) and (17) have been studied as a function of energy. The relative topological cross sections have been calculated, and the fraction of elastic-scattering events is seen to drop sharply as energy increases. We have calculated the average charged-particle multiplicities in inelastic events and compared them with those for other reactions in terms of a simple model. Good agreement is found with results at higher energies, although threshold effects must be considered here. In particular, the average multiplicities for $\pi^+\pi^-$ and $\pi^-\pi^-$ reactions are essentially equal and higher than those of all other (on-shell) hadron-hadron reactions at a given energy.

We have also presented inclusive distributions

TABLE V. Averaged-charged-particle-multiplicity fit parameters. Results of fits to $\langle n_X \rangle = A + B \ln(s/8)$.

Reaction	s range (GeV^2)	Number of points	A	B	χ^2/NDF
$\pi^-\pi^-$	1.6–6.6	4	3.14 ± 0.06	0.57 ± 0.06	3.4
$\pi^+\pi^-$	0.8–5.9	5	3.16 ± 0.04	1.00 ± 0.03	15.3
pp	9.5–26	8	2.34 ± 0.03	1.00 ± 0.04	4.1
π^+p	8.4–29	7	3.04 ± 0.02	1.08 ± 0.04	1.6
π^-p	8.4–25	8	2.57 ± 0.06	1.16 ± 0.07	0.8
K^+p	6.8–24	6	2.68 ± 0.02	0.99 ± 0.04	1.8
K^-p	16.7–29	3	2.37 ± 0.09	1.13 ± 0.09	0.002

TABLE VI. $d\sigma/dp_T^2$ slopes in $\pi\pi$ interactions. Results of fits to $d\sigma/dp_T^2 = Ae^{-bp_T^2}$.

Reaction	M_X^2 range (GeV^2)	p_T^2 range [(GeV/c)^2]	b [(GeV/c)$^{-2}$]
$\pi^-\pi^- \to \pi^- + X$	0.0–2.5	0.00–0.24	8.69 ± 0.45
		0.24–0.64	5.24 ± 0.69
	2.5–4.0	0.00–0.24	9.71 ± 0.49
		0.24–0.70	4.74 ± 0.58
	4.0–5.5	0.00–0.24	9.64 ± 0.50
		0.24–0.70	3.87 ± 0.59
	5.5–max	0.00–0.20	11.61 ± 0.65
		0.20–0.70	6.33 ± 0.56
$\pi^+\pi^- \to \pi^- + X$	0.00–1.25	0.00–0.70	14.69 ± 0.35
	1.25–2.50	0.00–0.70	9.76 ± 0.24
	2.50–3.75	0.00–0.16	11.19 ± 0.69
		0.16–0.70	6.45 ± 0.43
	3.75–5.00	0.00–0.24	9.80 ± 0.49
		0.24–0.70	7.30 ± 0.51
	5.00–max	0.00–0.12	11.49 ± 1.32
		0.12–0.70	7.47 ± 0.50
$\pi^+\pi^- \to \pi^- + X$	0.00–1.25	0.00–0.56	14.89 ± 0.39
	1.25–2.50	0.00–0.70	9.75 ± 0.22
	2.50–3.75	0.00–0.20	10.47 ± 0.52
		0.20–0.70	6.48 ± 0.53
	3.75–5.00	0.00–0.20	11.91 ± 0.63
		0.20–0.70	7.06 ± 0.45
	5.00–max	0.00–0.20	10.55 ± 0.73
		0.20–0.70	6.90 ± 0.50

TABLE VII. Elastic-scattering $d\sigma/dt$ fit parameters. Results of fits to $(1/\sigma_T)\, d\sigma/d|t| = Ae^{-b|t|}$.

M_X^2 range (GeV^2)	$\|t\|$ range [(GeV/c)^2]	A [(GeV/c)$^{-2}$]	b [(GeV/c)$^{-2}$]
	$\pi^-\pi^- \to \pi^-\pi^-$		
0.0–2.5	0.0–0.4	1.91 ± 0.21	4.60 ± 0.65
	0.0–0.6	1.73 ± 0.18	3.82 ± 0.43
	0.0–1.0	1.38 ± 0.12	2.63 ± 0.23
2.5–4.0	0.0–0.7	0.92 ± 0.15	5.19 ± 0.73
	0.0–1.0	0.83 ± 0.13	4.60 ± 0.56
4.0–5.5	0.0–0.4	0.84 ± 0.18	7.78 ± 1.50
	0.0–1.0	0.59 ± 0.12	5.05 ± 0.80
5.5–max	0.0–1.0	0.34 ± 0.11	6.54 ± 1.75
	$\pi^+\pi^- \to \pi^+\pi^-$		
0.00–1.25	0.0–0.3	3.10 ± 0.23	6.74 ± 0.55
	0.0–1.0	2.02 ± 0.10	3.54 ± 0.14
	0.0–1.4	1.93 ± 0.10	3.35 ± 0.12
1.25–2.50	0.0–0.6	0.91 ± 0.10	5.39 ± 0.46
	0.0–1.2	0.47 ± 0.05	2.72 ± 0.18
2.50–3.75	0.0–0.4	0.92 ± 0.16	8.96 ± 1.08
	0.0–0.8	0.65 ± 0.09	6.54 ± 0.48
	0.0–1.4	0.56 ± 0.08	5.86 ± 0.42
3.75–5.00	0.0–0.4	0.60 ± 0.12	6.52 ± 1.16
	0.0–0.8	0.55 ± 0.10	5.87 ± 0.87
5.00–max	0.0–0.4	0.16 ± 0.05	4.56 ± 1.60
	0.0–0.8	0.14 ± 0.04	3.71 ± 1.16

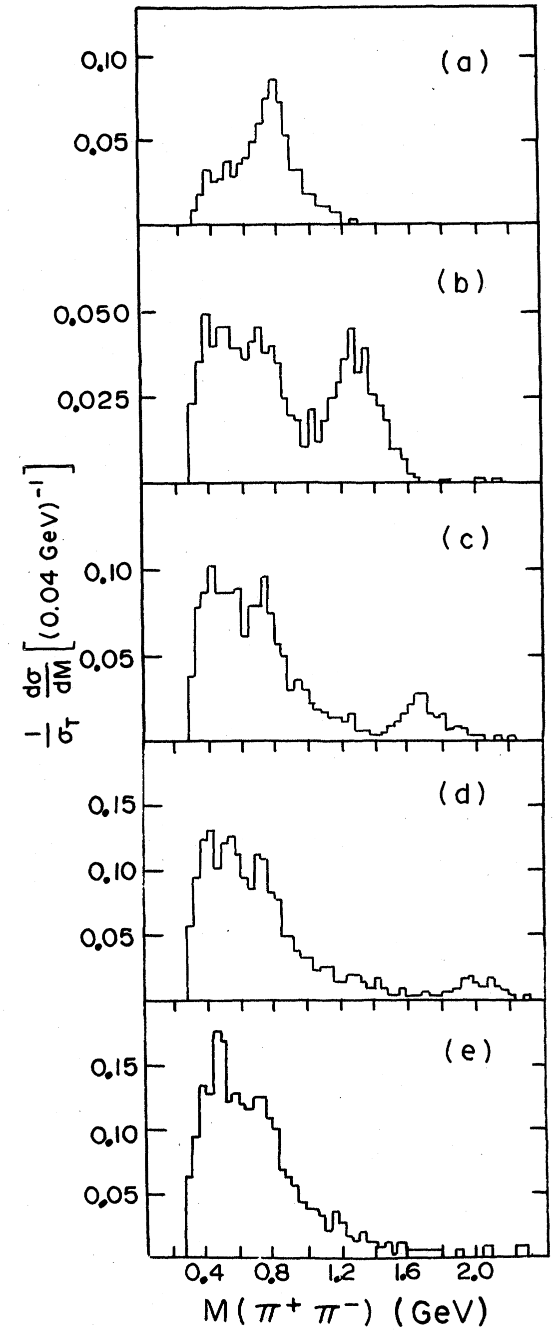

FIG. 20. $\pi^+\pi^-$ effective-mass distributions for $\pi^+\pi^- \to \pi^+\pi^- + X'$ for (a) $M_X^2 < 1.25$ GeV^2, (b) $1.25 < M_X^2 < 2.50$ GeV^2, (c) $2.50 < M_X^2 < 3.75$ GeV^2, (d) $3.75 < M_X^2 < 5.00$ GeV^2, (e) $M_X^2 > 5.00$ GeV^2.

in x and p_T^2 for particles produced in $\pi\pi$ interactions. The x distributions show the expected symmetries, with leading peaks due entirely to elastic scattering. The exponential slopes of the p_T^2 distributions have been found to have a break near $p_T^2 \simeq 0.25$ (GeV/c)^2 (except for $\pi^+\pi^-$ interactions

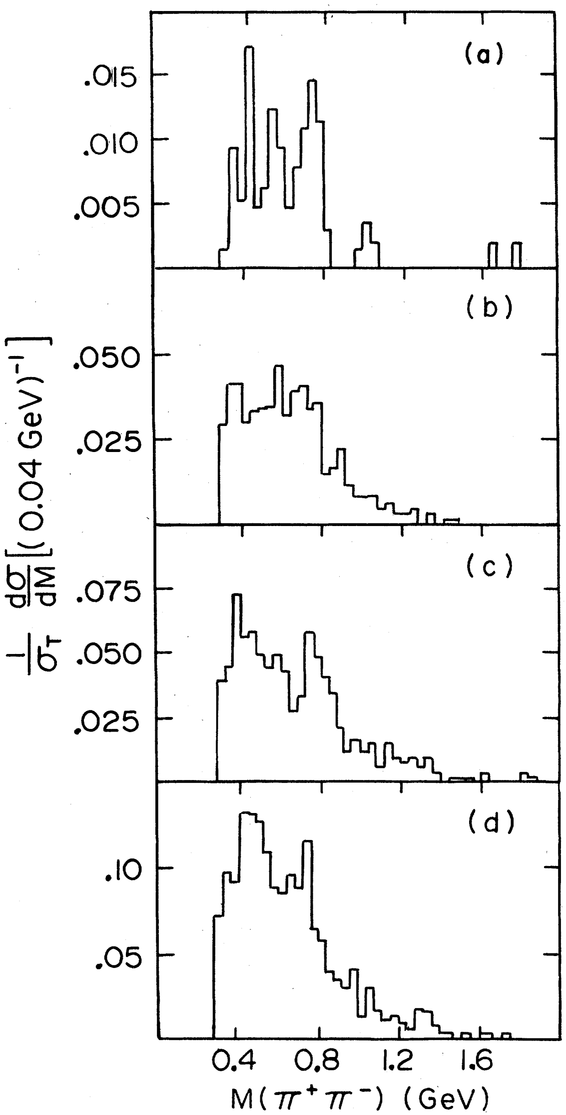

FIG. 21. $\pi^+\pi^-$ effective-mass distributions for $\pi^-\pi^- \rightarrow \pi^+\pi^- + X'$ for (a) $M_X{}^2 < 2.5$ GeV^2, (b) $2.5 < M_X{}^2 < 4.0$ GeV^2, (c) $4.0 < M_X{}^2 < 5.5$ GeV^2, (d) $M_X{}^2 > 5.5$ GeV^2.

dominated by s-channel resonance production), in general agreement with other interactions. Evidence of ρ^0 production is found at all energies studied. We have also presented $d\sigma/dt$ distributions for elastic scattering which show evidence of shrinkage of the diffraction peak in $\pi^-\pi^-$ interactions.

Thus, we find that pion-pion interactions are generally very similar to other hadron-hadron interactions. Indeed, the qualitative features of pion-pion interactions reveal nothing that has not been found in other interactions. Quantitatively, however, we have found differences, particularly in the average multiplicities.

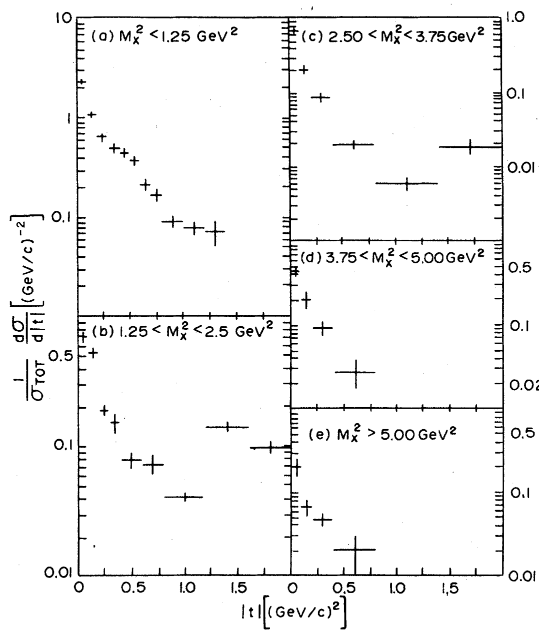

FIG. 22. t distributions for $\pi^+\pi^- \rightarrow \pi^+\pi^-$ for (a) $M_X{}^2 < 1.25$ GeV^2, (b) $1.25 < M_X{}^2 < 2.50$ GeV^2, (c) $2.50 < M_X{}^2 < 3.75$ GeV^2, (d) $3.75 < M_X{}^2 < 5.00$ GeV^2, (e) $M_X{}^2 > 5.00$ GeV^2.

ACKNOWLEDGMENTS

This work was supported in part by the U. S. Department of Energy under Contract No. DE-

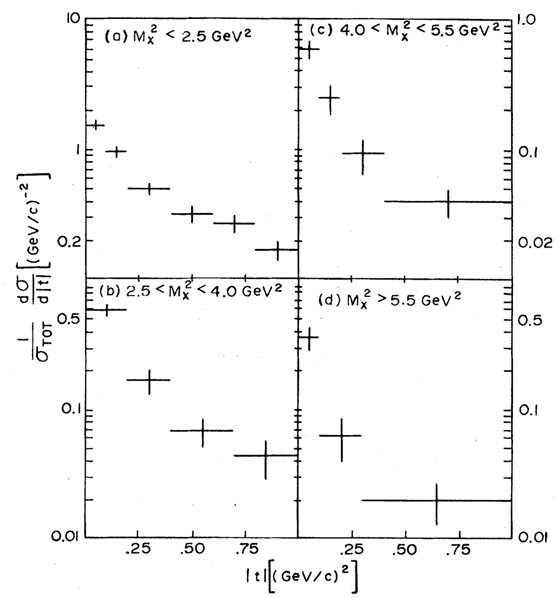

FIG. 23. t distributions for $\pi^-\pi^- \rightarrow \pi^-\pi^-$ for (a) $M_X{}^2 < 2.5$ GeV^2, (b) $2.5 < M_X{}^2 < 4.0$ GeV^2, (c) $4.0 < M_X{}^2 < 5.5$ GeV^2, (d) $M_X{}^2 > 5.5$ GeV^2.

ACO2-76ERO3069. We wish to thank SLAC and the operating crew of the 82-in. bubble chamber for providing the film for this experiment, as well as the scanning and measuring technicians of Columbia University and MIT for their fine efforts. We particularly acknowledge the assistance of Professor Charles Baltay and Dr. Mohan Kalelkar for providing the $\pi^{+}p$ data.

---

*Present address: DESY, Hamburg, West Germany.
†Permanent address: Tel-Aviv University, Ramat-Aviv, Israel.
‡Present address: Tufts University, Medford, Massachusetts.
§Present address: Rockefeller University, New York, New York.
||Present address: Automatix, Burlington, Massachusetts.
¶Present address: Bell Laboratories, Naperville, Illinois.

[1]G. Chew and F. Low, Phys. Rev. 113, 1640 (1959).
[2]See, for example, H. P. Dürr and H. Pilkuhn, Nuovo Cimento 40A, 899 (1965); E. Ferrari and F. Selleri, *ibid.* 27, 1450 (1963); G. Wolf, Phys. Rev. Lett. 19, 925 (1967); J. Benecke and H. P. Dürr, Nuovo Cimento 56A, 269 (1968).
[3]S. J. Barish *et al.*, Phys. Rev. D 12, 1260 (1975).
[4]F. Barreiro *et al.*, Phys. Rev. D 17, 681 (1978).
[5]J. Erwin *et al.*, Phys. Rev. Lett. 35, 980 (1975).
[6]J. de Brion *et al.*, Phys. Rev. Lett. 34, 910 (1975).
[7]F. Barreiro *et al.*, Phys. Rev. Lett. 40, 595 (1978).
[8]D. Brick *et al.*, Phys. Rev. D 18, 3099 (1978).
[9]F. Barreiro *et al.*, internal memorandum (unpublished).
[10]W. J. Robertson *et al.*, Phys. Rev. D 7, 2554 (1973).
[11]M. S. Kalelkar, Ph.D. thesis, Columbia University, 1975 (unpublished).
[12]P. C. Trepagnier, Ph.D. thesis, MIT., 1975 (unpublished).
[13]J. P. Silverman, Ph.D. thesis, MIT, 1978 (unpublished).
[14]P. L. Bastien *et al.*, Phys. Rev. D 3, 2047 (1971).
[15]R. A. Singer, Ph.D. thesis, MIT, 1972 (unpublished).
[16]E. Gotsman, Phys. Rev. D 9, 1575 (1974).
[17]E. Bracci *et al.*, CERN Report No. CERN/HERA/73-1, 1973 (unpublished).
[18]E. Bracci *et al.*, CERN Report No. CERN/HERA/72-1, 1972 (unpublished).
[19]E. Bracci *et al.*, CERN Report No. CERN/HERA/72-2, 1972 (unpublished).
[20]W. R. Frazer *et al.*, Rev. Mod. Phys. 44, 284 (1972).
[21]D. Brick *et al.*, Phys. Rev. D 19, 743 (1979).
[22]E. Albini *et al.*, Nuovo Cimento 32A, 101 (1976).
[23]Proportional Hybrid System Consortium, Phys. Rev. Lett. 45B, 136 (1973).
[24]P. Schmid, CERN Report No. CERN/EP/PHYS 76-57, 1976 (unpublished).
[25]E. Shrauner, Phys. Rev. Lett. 20, 1258 (1968).